A schistosome β subunit remodels inactivation of a calcium channel *via* an N-terminal polyacidic motif

Vicenta Salvador-Recatala & Robert M. Greenberg

Department of Pathobiology, School of Veterinary Medicine, University of Pennsylvania, Philadelphia, PA 19104

The β subunit of high voltage-activated Ca^{2+} (Ca_v) channels targets the pore forming α_1 subunit to the plasma membrane and defines the biophysical phenotype of the Ca_v channel complex[1-2]. Ca_v channel inactivation following activation and opening is tightly regulated and is an essential property that not only prevents excessive entry of Ca^{2+} into the cell but may also have functions in signal transduction[3]. The β subunit modulates Ca^{2+}-dependent and voltage-dependent components of Ca_v channel inactivation *via* its interaction with the I-II linker of the α_1 subunit[4-5]. Here, using Ca_v2.3 and whole-cell patch-clamp, we show that a β subunit from the human parasite *Schistosoma mansoni* (β_{Sm}) accelerates inactivation *via* a unique, long <u>N</u>-terminal <u>p</u>oly<u>a</u>cidic <u>m</u>otif (NPAM). The accelerating effect of NPAM-containing subunits, both native β_{Sm} and chimeric mammalian β_{1b}, β_{2a} and β_3 subunits to which NPAM had been attached, was only apparent when Ca^{2+} was internally buffered with BAPTA (5 mM) or when Ba^{2+} was used as the charge carrier, two commonly used strategies to eliminate Ca^{2+}/calmodulin dependent inactivation. These results indicate that calmodulin is not involved. In addition to accelerating inactivation, NPAM-containing β subunits significantly reduced current density with respect to their non NPAM-bearing counterparts. Interestingly, when the amino acids N terminal to NPAM were deleted, inactivation of Ca_v2.3 currents was faster than in the presence of the entire N-terminal portion of the β_{Sm} subunit, as if the pre-NPAM region counteracts the effect of NPAM. Presence of NPAM also resulted in currents that activated faster, suggesting that NPAM increases open channel probability. However, NPAM does not modulate inactivation gating. In summary, this study identifies a structural determinant of Ca_v channel inactivation that is entirely unlike those previously known.

Fast inactivation of the Ca_v2.3 channel has a Ca^{2+}/calmodulin-dependent component that is manifest when intracellular buffering is reduced to minimum, physiological levels[6-7]. Therefore, in the presence of mild buffering of intracellular Ca^{2+}, Ca_v2.3 inactivates by a Ca^{2+}-independent mechanism, which remains incompletely understood. In this study we compare currents produced in three different intracellular buffering conditions: no chelators (which presumably is comparable to the use of 20 μM EGTA[7]), "physiological" buffering with 0.5 mM EGTA[6], and strong buffering with 5 mM BAPTA[6-7]. Whole-cell currents produced by HEK cells stably expressing $Ca_v2.3$ and dialyzed with non-chelating solution, which allows accumulation of intracellular Ca^{2+}, inactivate significantly faster than currents from cells dialyzed with 0.5 mM EGTA, and these inactivate faster than with 5 mM BAPTA (Fig. 1a). In all buffering conditions, currents were optimally fitted by 2-exponential functions that presumably represent fast and slow components of inactivation. The fast component of inactivation in the presence of BAPTA was significantly larger (i.e., slower) than that displayed in the absence of buffers or in the presence of 0.5 mM EGTA. The fast component of inactivation in the presence of 0.5 mM EGTA was significantly slower than when no chelators were added (Fig. 1b). This result suggests that 0.5 mM EGTA partially chelates the Ca^{2+} signal produced by $Ca_v2.3$ channels alone. Consistent with these kinetic values, the fast component of inactivation contributed less to total inactivation in the presence of intracellular buffering than in its absence (Fig. 1d). The time constant of the slow component of inactivation was less affected by the intracellular buffering conditions (Fig. 1c), consistent with the notion that the slow component of inactivation in $Ca_v2.3$ is largely Ca^{2+}-independent.

When $Ca_v2.3$ was coexpressed with the β subunit from *S. mansoni* that most resembles mammalian β subunits[8-9], the kinetics of the fast component of inactivation of $Ca_v2.3$ appeared resistant to intracellular chelation ($p > 0.05$, 1-way ANOVA; Fig. 2a left). However, in the presence of β_{1b} and β_{2a} (but not β_3), this same fast inactivating component was significantly slowed by 5 mM BAPTA ($p < 0.001$, 1-way ANOVA with Bonferroni post-test; Fig. 2b-d, left), consistent with a previous report using β_{2a}[6]. In a search for structures that could be responsible for this phenomenon, we identified an uncharacterized long N-terminal poly-acidic motif in β_{Sm} ($NPAM_{30-44}$, Table 1) that does not occur in mammalian β subunits. As a first approach to test whether $NPAM_{30-44}$ was responsible for this apparent insensitivity of τ_{fast} to BAPTA, we generated a mutant of β_{Sm} that lacks the NPAM-encompassing first 44 amino acids ($\beta_{Sm\Delta 2-44}$), and complementary mutant mammalian β subunits to which this N-terminal region of β_{Sm} was attached, thus producing chimeric schistosome/mammalian β subunits. Coexpression with $\beta_{Sm\Delta 2-44}$, which lacks NPAM, resulted in a recovery of the sensitivity of the fast component of inactivation to 5 mM intracellular BAPTA (Fig. 2a, right). The reverse experiment corroborates this result, as coexpression with chimeric schistosome/mammalian β subunits, which contain NPAM, masked the sensitivity of inactivation to intracellular BAPTA (Fig. 2b-d, right). The acceleration of the fast component of inactivation by NPAM in the presence of BAPTA was concomitant with an increase in its contribution to total inactivation (Suppl. Fig. 1). Presence of NPAM also accelerated the slow kinetic component of inactivation when intracellular 5 mM BAPTA was used (Suppl. Fig. 2). Because BAPTA eliminates Ca^{2+}-dependent inactivation of $Ca_v2.3$ channels[6], these data suggest that NPAM accelerates an inactivating process that is Ca^{2+}-independent, putatively voltage-dependent inactivation (VDI). Ba^{2+} currents also inactivated significantly faster in the presence of NPAM-containing β subunits than in the presence of NPAM-lacking β subunits (Fig. 3), which rules out the involvement of calmodulin[10]. In contrast to Ca^{2+} currents, when Ba^{2+} was used as the charge carrier, NPAM did not significantly accelerate the slow component of inactivation, except in the case of β_{2a} (Fig. 3, right side of the panels) . Since polyacidic clusters in other voltage-gated ion channels are involved in

Ca^{2+} binding[11-12], a model in which a putative BAPTA-refractory, Ca^{2+}-sensing function of NPAM leads to fast inactivation cannot be excluded. The reduction of Ca^{2+} (or substitution of Ba^{2+}) would unmask this putative property of NPAM that ordinarily cannot be seen due to overriding the effects of CDI.

Whole-cell currents from cells co-expressing N-terminally truncated β_{Sm} were smaller than those produced in the presence of wild-type β_{Sm}. Averaged current density-voltage plots of β_{Sm} as well as chimeric mammalian β subunits show that this difference was significant in all cases except for β_{1b} (Fig. 4). Thus, the N-terminus of β_{Sm} appears to be multifunctional, with roles in inactivation kinetics and determining levels of current density, as well as in current run-down, as we have previously described[13]. To determine whether different regions of the N-terminus of β_{Sm} are responsible for accelerating inactivation and modulating current density, two additional mutant versions of β_{Sm} were generated: $\beta_{Sm\Delta 2\text{-}17}$, which lacks the first 17 amino acids, and $\beta_{Sm\Delta 2\text{-}24}$, which additionally lacks a short acidic motif, at position 18-24 (Fig. 5a). Both of these constructs leave the longer, NPAM region intact. Interestingly, Ba^{2+} currents inactivated faster in the presence of either deletion mutant ($\beta_{Sm\Delta 2\text{-}17}$ or $\beta_{Sm\Delta 2\text{-}24}$) than in the presence of the wild type subunit (Fig. 5b), suggesting that the region of β_{Sm} N-terminal to NPAM somehow moderates the accelerating effect of NPAM on inactivation kinetics. Kinetic analyses show that the fast component of inactivation was especially affected by these deletions (Fig. 5c, d). Our finding that shortening the length of the β subunit N-terminus accelerates inactivation contrasts with previous studies showing that inactivation rate is increased by the presence of a longer β subunit N-terminus, regardless of the amino acid composition[14-15]. We also found that the pre-NPAM segment has no effect on current density (Fig. 5e). The short tyrosine-containing acidic motif at position 18-24 of β_{Sm} appears to play no role in inactivation or current density, but perhaps it is relevant to membrane association, by analogy with the motif EEEEDYEEE in the C-terminus of β_{1b}[16].

Another interpretation is that NPAM accelerates inactivation of $Ca_v2.3$ by interacting with structures that mediate VDI. The molecular mechanisms and structures involved in VDI of Ca_v channels are, however, incompletely understood. Using hybrid Ca_v channels that contain parts of rat $Ca_v2.1$ and parts of marine ray $Ca_v2.3$, it appears that the S6 segments of all four domains of $Ca_v2.3$ are relevant to VDI via constriction of the pore[17-18]. However, because the I-II linker largely contributes to determining the rate of inactivation, an alternative model has been proposed in which the I-II linker functions as a hinged lid, or inactivation ball, which docks at domain II, III, or both[5]. Since the β subunit interacts with the AID motif on the I-II linker[19], β subunits might have a function as part of the hinged lid, with perhaps the β subunit N-terminus as an important structure in this model, especially because its size appears to correlate with its ability to induce fast inactivation[14-15]. Interestingly, domain III of $Ca_v2.3$ is involved in both inactivation kinetics and inactivation gating, but domain II appears to determine inactivation kinetics exclusively[5]. According to a model proposed by Aldrich and collaborators[19-20], a slowing in macroscopic inactivation may be the result of a delay in channel opening at the single channel level. Therefore, if channel opening is delayed, many channels would open while the channel inactivates, thus slowing macroscopic inactivation, and vice versa. Indeed, we observed faster activation of the currents when NPAM was present (see current traces in Figs. 2 and 3). Fitting the activating portion of the inward currents to single exponential functions yielded time constants of activation (τ_{act}) for all channel combinations. In all cases, τ_{act} was smaller (faster activation) in the presence of the NPAM-bearing β subunits than in the presence of the corresponding β subunit without NPAM, in agreement with this model. In the case of β_{2a} and β_3, this difference was statistically significant (Table 2). Therefore, NPAM could also induce fast inactivation but promoting fast channel opening.

Since some structures of Ca_v channels are involved in both inactivation kinetics and inactivation gating, we wanted to know whether the N-terminus of β_{Sm} would also affect inactivation gating. To this end, we applied a steady-state inactivation voltage protocol to Ca_v2.3-HEK cells expressing NPAM-containing β subunits or NPAM-lacking subunits. Whereas the midpoint of steady-state inactivation is also Ca^{2+}-dependent, and remodelled by β subunits (Suppl. Fig. 3) -consistent with the notion that Ca^{2+}-dependent inactivation inhibits channel opening induced by depolarization from a resting potential[4]- the presence of the NPAM-containing N-terminus of β_{Sm} did not modulate steady-state inactivation under any intracellular buffering scenario. Figure 6 compares steady-state inactivation in the presence of 5 mM BAPTA. If NPAM interacts directly with structures that specifically determine inactivation kinetics, domain II appears to be a good candidate, as it does not affect inactivation gating[5].

In summary, we have identified a structural determinant of Ca_v channel inactivation that greatly differs from those previously known. This structure is a long poly-acidic motif in the N-terminus of a Ca_v β subunit that, to date appears exclusively in parasitic flatworms (Table 1). We hypothesize that the effects of this structure on inactivation and current density represent a mechanism that restricts Ca^{2+} entry and ensures the viability of the parasite. Disruption of this unique mechanism for maintenance of Ca^{2+} homeostasis may provide a useful strategy for new antihelminthic therapies.

$Ca_v2.3$ voltage-gated Ca^{2+} channels play important roles in synaptic transmission[21-24], secretion[25-26] and long-term potentiation[27]. $Ca_v2.3$ functionally interacts with many β subunits in heterologous expression systems[28-29]. Given the portability of the NPAM function onto mammalian β subunits and the potential of β subunits as targets for genetic therapy[30], NPAM might become useful to reduce excessive Ca^{2+} and/or exocytosis in pathological conditions such as ischemia.

Methods Summary

Cell culture and transfection. HEK cells stably expressing the $Ca_v2.3$ channel were cultured as previously described[13]. Cells were transiently transfected with β constructs using the calcium phosphate method.

DNA constructs. Using standard methods, we cloned all β subunits into the pXOOM vector[31] which contains the gene for green fluorescent protein (GFP) as a marker for transfection.

Construction of β chimeras. Chimeric β_{Sm} /mammalian β subunits were created by first amplifying by PCR the amino terminal region of β_{Sm} (corresponding to amino acids 1-63) and the coding region of the mammalian β subunits, using primers with appropriate restriction sites. The amplified regions were purified, digested with restriction enzymes, and ligated together. The sites in the mammalian β subunits at which the NPAM was added correspond to amino acid #7 for β_{1b}, amino acid #9 for β_{2a}, and amino acid #6 for β_3. Chimeric constructs were ligated into the pXOOM vector. The β_{2a} chimera maintained the two N-terminal cysteine residues required for palmitoylation[32].

Electrophysiology. We performed whole-cell patch-clamp of HEK cells stably transfected with $Ca_v2.3$.

Full methods accompany this paper.

References

1. Hidalgo, P. & Neely, A. Multiplicity of protein interactions and functions of the voltage-gated calcium channel beta-subunit. *Cell Calcium* **42,** 389-396 (2007).

2. Dolphin, A.C. Calcium channel diversity: multiple roles of calcium channel subunits. *Curr Opin Neurobiol* **19,** 237-244 (2009).

3. Morad, M. & Soldatov, N. Calcium channel inactivation: Possible role in signal transduction and Ca^{2+} signalling. *Cell Calcium* **38**, 223-231 (2005).

4. Cens, T., Rousset, M., Leyris, J.P., Fesquet, P. and Charnet, P. Voltage- and calcium-dependent inactivation in high voltage-gated Ca^{2+} channels. *Prog Biophys Mol Biol* **90,** 104-117 (2006).

5. Stotz, S.C., Hamid, J., Spaetgens, R.L., Jarvis, S.E. & Zamponi, G.W. Fast inactivation of voltage-dependent calcium channels. *J Biol Chem* **275,** 24575-24582 (2000).

6. Liang, H., DeMaria, C.D., Erickson, M.G., Mori, M.X., Alseikhan, B.A. & Yue, D.T. Unified mechanisms of Ca^{2+} regulation across the Ca^{2+} channel family. *Neuron* **39,** 951-960 (2003).

7. Leroy, J., Pereverzev, A., Vajna, R., Pfitzer, G., Hescheler, J., Malécot, C.O., Schneider, T. & Klöckner, U. Ca^{2+} -sensitive regulation of E-type Ca^{2+} channel activity depends on an arginine-rich region in the cytosolic II-III loop. *Eur J Neurosci* **18**, 841-855 (2003).

8. Kohn, A.B., Anderson, P.A., Roberts-Misterly, J.M. & Greenberg, R.M. Schistosome calcium channel beta subunits. Unusual modulatory effects and potential role in the action of the antischistosomal drug praziquantel. *J Biol Chem* **276**, 36873-36876 (2001).

9. Jeziorski, M.C. & Greenberg, R.M. Voltage-gated calcium channel subunits from platyhelminths: potential role in praziquantel action. *Int J Parasitol* **36**, 625-632 (2006).

10. Chao, S.-H., Suzuki, Y., Zysk, J.R. & Cheung, W.Y. Activation of calmodulin by various metal cations as a function of ionic radius. *Mol Pharmacol* **26,** 75-82 (1984).

11. Xiao, Q., Prussia, A., Yu, K., Cui, Y.Y. & Hartzell, H.C. Regulation of bestrophin Cl channels by calcium: role of the C terminus. *J. Gen. Physiol.* **132**, 681-692 (2008).

12. Schreiber, M. & Salkoff, L. A novel calcium-sensing domain in the BK channel. *Biophys. J.* **73**, 1355-1363 (1997).

13. Salvador-Recatala, V., Schneider, T. & Greenberg, R.M. Atypical properties of a conventional calcium channel beta subunit from the platyhelminth *Schistosoma mansoni*. BMC Physiol **8**, 6 (2008).

14. Herzig, S., Khan, I.F.Y., Gründenmann, D., Matthes, J., Ludwig, A., Michels, G., Hoppe, U.C., Chaudhuri, D., Schwartz, A., Yue, D.T. & Hullin, R. Mechanism of Cav1.2 channel modulation by the amino terminus of cardiac β_2-subunits. *FASEB J* **21,** 1527-1538 (2007).

15. Jangsangthong, W., Kuzmenkina, E., Khan, I.F.Y., Matthes, J., Hullin, R. & Herzig, S. Inactivation of L-type calcium channels is determined by the length of the N terminus of mutant β_1 subunits. *Pflugers Arch* (Epub ahead of print).

16. Bogdanov, Y., Brice, N.L., Canti, C., Page, K.M., Li, M., Volsen, S.G. & Dolphin, A.C. Acidic motif responsible for plasma membrane association of the voltage-dependent calcium channel β1b subunit. *Eur J Neurosci* **12,** 894-902 (2000).

17. Zhang, J.F., Ellinor, P.T., Aldrich, R.W. and Tsien, R.W. Molecular determinants of voltage-dependent inactivation in calcium channels. *Nature* **372,** 97-100 (1994).

18. Spaetgens, R.L. & Zamponi, G.W. Multiple structural domains contribute to voltage-dependent inactivation of rat brain α_{1E} calcium channels. *J Biol Chem* **274,** 22428-22436 (1999).

19. Aldrich, R.W., Corey, D.P. & Stevens, C.F. A reinterpretation of mammalian sodium channel gating based on single channel recording. *Nature* **306,** 436-441 (1983).

20. Aldrich, R.W. & Stevens, C.F. Voltage-dependent gating of single sodium channels from mammalian neuroblastoma cells. *J Neurosci* **7,** 418-431 (1987).

21. Gasparini, S., Kasyanov, A.M., Pietrobon, D., Voronin, L.L & Cherubini, E. Presynaptic R-type calcium channels contribute to fast excitatory synaptic transmission in the rat hippocampus. *J Neurosci* **21,** 8715-8721 (2001).

22. Kamp, M.A., Krieger, A., Henry, M., Hescheler, J., Weiergraber, M. & Schneider, T. Presynaptic "$Ca_v2.3$-containing" E-type Ca^{2+} channels share dual roles during neurotransmitter release. *Eur J Neurosci* **21,** 1617-1625 (2005).

23. Wu, L.-G., Borst, J.G. & Sakmann, B. R-type Ca^{2+} currents evoke transmitter release at a rat central synapse. *Proc Natl Acad Sci USA* **95,** 4720-4725 (1998).

24. Castro, A., Andrade, A., Vergara, P., Segovia, J., Aguilar, J., Felix, R. & Delgado-Lezama, R. Involvement of R-type Ca^{2+} channels in neurotransmitter release from spinal dorsolateral funiculus terminals synapsing motoneurons. *J Comp Neuro* **513,** 188-196 (2009).

25. Albillos, A., Neher, E. & Moser, T. R-type Ca^{2+} channels are coupled to the rapid component of secretion in mouse adrenal slice chromaffin cells. *J. Neurosci* **20,** 8323-8330 (2000).

26. Wang, G., Dayanithi G., Newcomb, R. & Lemos, J.R. An R-type Ca^{2+} current in neurohypophysial terminals preferentially regulates oxytocin secretion. *J Neuroscience* **19,** 9235-9241 (1999).

27. Dietrich, D., Kirschstein, T., Kukley, M., Pereverzev, A., von der Brelie, C., Schneider, T. & Beck, H. Functional specialization of presynaptic $Ca_v2.3$ Ca^{2+} channels. *Neuron* **39,** 483-496 (2003).

28. Jones, L.P., Wei, S.-K. & Yue, D.T. Mechanism of auxiliary subunit modulation of neuronal α_{1E} calcium channels. *J. Gen. Physiol.* **112,** 125-143 (1998).

29. Parent, L., Schneider, T., Moore, C.P. & Talwar, D. Subunit regulation of the human brain alpha 1E calcium channel. *J Membr Biol* **160,** 127-140 (1997).

30. Cingolani, E., Ramirez Correa, G.A., Kizana, E., Murata, M., Cho, H.C. & Marban, E. Gene therapy to inhibit the calcium channel β subunit. *Circulation Research* **101,** 166-175 (2007).

31. Jespersen, T., Grunnet, M., Angelo, K., Klaerke, D.A. & Olesen, S.P. Dual-function vector for protein expression in both mammalian cells and *Xenopus laevis* oocytes. *Biotechniques* **32,** 536-540 (2002).

32. Chien, A.J., Carr, K.M., Shirokov, R.E., Rios, E., & Hosey, M.M. Identification of palmitoylation sites within the L-type calcium channel β_{2a} subunit and effects on channel function. *J. Biol. Chem.* **271**, 26465-26468 (1996).

We thank Dr. Toni Schneider for the HEK cell line stably expressing human $Ca_v2.3$, Dr. Diane Lipscombe for the β_3 subunit, Dr. Annette Dolphin for the β_{1b} subunit, and Dr. Richard Horn and Dr. Ji-Fang Zhang for critical reading. We thank William Morgan for technical assistance. This work was supported by NIH grants AI 40522 and AI 73660.

The author's declare no competing interests.

V.S.R. designed the research, performed experiments, analyzed the data, discussed the results and wrote the manuscript. R.M.G. performed experiments, discussed results, provided suggestions for experiments, and contributed to the manuscript.

Correspondence and requests for materials should be addressed to V.S.R. (vicenta@vet.upenn.edu).

LEGENDS

FIGURE 1. **Ca^{2+}-dependent inactivation of $Ca_v2.3$ is suppressed by mild chelation.** **a,** $Ca_v2.3$ currents elicited by a depolarizing pulse to +30 mV from a holding potential of -80 mV in the absence of internal chelators and in the presence of 0.5 mM EGTA or 5 mM BAPTA. **b,** Average values for the fast (predominant) time constant of inactivation (τ_{fast}) for $Ca_v2.3$ in zero internal chelation (open bar), 0.5 mM EGTA (grey) and 5 mM BAPTA (black). **c**, Average values of the slow time constant of inactivation (τ_{slow}) for $Ca_v2.3$ in zero internal chelation, 0.5 mM EGTA (grey), and 5 mM BAPTA (black). **d,** Percentage

contribution of the fast component of inactivation to total inactivation in zero internal chelation (open bar), 0.5 mM EGTA (grey) and 5 mM BAPTA (black). **e,** Percentage contribution of the slow component of inactivation to total inactivation in zero internal chelation (open bar), 0.5 mM EGTA (grey) and 5 mM BAPTA (black). Bars represent mean ± s.e.m. ** P < 0.01, One-way ANOVA with Bonferroni post-test (n = 4-16).

FIGURE 2. β subunits with N-terminal poly-acidic motif (NPAM) accelerate the fast component of inactivation of Ca^{2+} currents produced by $Ca_v2.3$ when the intracellular solution contains 5 mM BAPTA.

a-d, Whole-cell $Ca_v2.3$ currents elicited by a depolarizing pulse to maximum peak current from a holding potential of -80 mV in the presence of internal 5 mM BAPTA with the following coexpressed β subunits: β_{Sm} or the N-terminally deleted $\beta_{Sm\Delta2\text{-}44}$ (**a**), β_{1b} or the chimera NPAM-β_{1b} (**b**), β_{2a} or the chimera NPAM-β_{2a} (**c**), β_3 or the chimera NPAM-β_3 (**d**). Current amplitudes are normalized to highlight the differences in inactivation kinetics. Plotted below the current traces are average values of the fast time constant (τ) of macroscopic inactivation for $Ca_v2.3$ channels coexpressed with wild type and modified β subunits for each intracellular buffering milieu. The fast τ was derived by 2-exponential fits of the inactivating portions of Ca^{2+} currents produced by HEK cells dialyzed with non-chelated solution (open bars) or with solution containing 0.5 mM EGTA (grey bars) or 5 mM BAPTA (black bars). Bars represent mean ± s.e.m. *P < 0.05, **P < 0.01, ***P < 0.001 (asterisks above bars), One-way ANOVA with Bonferroni post-test (n = 3-13). Stars within bars indicate statistically significant difference between wild-type and modified β subunits for the same intracellular buffering milieu; *P < 0.05, **P < 0.01, ***P < 0.001, unpaired Student's t-test. Welch’s corrections were applied when the variances were significantly different. Supplementary Table 1 shows average values for fast and slow time constants of inactivation for all channel subunit combinations under all three buffering conditions.

FIGURE 3. β subunits with N-terminal poly-acidic motif (NPAM) accelerate inactivation of Ba^{2+} currents produced by Ca_v2.3.

a-d, Whole-cell Ca_v2.3 currents elicited by a depolarizing pulse to maximum peak current from a holding potential of -80 mV in the presence of internal 5 mM BAPTA with the following coexpressed β subunits: β_{Sm} or the N-terminally deleted $\beta_{Sm\Delta2\text{-}44}$ (**a**), β_{1b} or the chimera NPAM-β_{1b} (**b**), β_{2a} or the chimera NPAM-β_{2a} (**c**), β_3 or the chimera NPAM-β_3 (**d**). Current amplitudes are normalized to highlight the differences in inactivation kinetics. Plotted below the current traces are average values of fast and slow time constants of macroscopic inactivation for Ca_v2.3 channels coexpressed with wild type and modified β subunits for each intracellular buffering milieu. Time constants of inactivation were derived by 2-exponential fits of the inactivating portions of Ba^{2+} currents produced by HEK cells. Bars represent mean ± s.e.m. * $P < 0.05$, **$P < 0.01$, ***$P < 0.001$, unpaired Student's t-test. Welch's corrections were applied when the variances were significantly different. Supplementary Table 2 shows average values for fast and slow time constants of inactivation for all channel subunit combinations using Ba^{2+} as the charge carrier. N = 3-7.

FIGURE 4. Current density is larger in the presence of N-terminal poly-acidic motif (NPAM)-bearing β subunits than in the presence of NPAM -lacking β subunits

a-d, Density of whole-cell $Ca_v2.3$ currents as a function of voltage. Depolarizing voltage-steps were delivered from a holding potential of -80 mV. Currents were recorded in the presence of the following coexpressed β subunits: β_{Sm} or the N-terminally deleted $\beta_{Sm\Delta2\text{-}44}$ (**a**), β_{1b} or the chimera NPAM-β_{1b} (**b**), β_{2a} or the chimera NPAM-β_{2a} (**c**), β_3 or the chimera NPAM-β_3 (**d**). Open circles represent data obtained with β subunits that naturally or artificially lack NPAM, filled circles represent data obtained with β subunits that naturally or artificially contain NPAM. Current density-voltage relationships for $Ca_v2.3$ channels expressed alone are also shown (squares) for a comparison. Data points represent mean ± s.e.m.

FIGURE 5. Deleting the N-terminal segment that precedes the NPAM of β_{Sm} accelerates macroscopic inactivation of $Ca_v2.3$ Ba^{2+} currents but does not influence current density.

a, Diagram showing the structure of the N-terminus of β_{Sm} and deleted versions that lack amino acids 2-17, amino acids 2-24 that contain a short polyacidic motif, and amino acids 2-44, which additionally lack the long polyacidic motif (NPAM). **b,** Comparison of macroscopic Ba^{2+} currents of $Ca_v2.3$ in the presence of the deletion mutants Δ2-17 or Δ2-24. **c-d,** Average values for the fast time constant of inactivation (**c**) and slow time constant of inactivation (**d**) for $Ca_v2.3$ in the presence of β_{Sm}Δ2-44 (open bars), wild type β_{Sm} (black bars), β_{Sm}Δ2-17 (grey bars), or β_{Sm}Δ2-24 (stripped bars). **e,** Current density-voltage relationships in the presence of β_{Sm}Δ2-17 (n = 9), β_{Sm}Δ2-24 (n = 7), or in the absence of β subunits (n = 3). See Fig. 4a for a comparison with wild type β_{Sm}. Data points represent mean ± s.e.m. One-way ANOVA with Bonferroni post-test, $*P < 0.05$, $**P < 0.01$, $***P < 0.001$. N = 3-7.

FIGURE 6. The N-terminus of β_{Sm} does not modulate steady-state inactivation of Ca_v2.3 channels.

a-d, Comparison between steady-state inactivation of Ca_v2.3, using Ca^{2+} as the charge carrier and 5 mM internal BAPTA for β_{Sm} (filled circles) and $\beta_{Sm\Delta2\text{-}44}$ (open circles) (**a**), for β_{1b} (open circles) and NPAM-β_{1b} (filled circles) (b), for β_{2a} (open circles) and NPAM-β_{2a} (filled circles), and for β_3 (open circles) and NPAM-β_3 (filled circles). Data points represent mean ± s.e.m. (n = 3-6). Solid lines represent Boltzmann fits to the data. Supplementary Table 3 shows average values for midpoints of steady-state inactivation for all channel subunit combinations under various internal buffering conditions.

SUPPLEMENTARY FIGURE 1. Percentage contribution of the fast component of macroscopic inactivation to total inactivation of Ca^{2+} currents of Ca_v2.3 is larger in the presence of N-terminal poly-acidic motif (NPAM)-bearing β subunits than in the presence of NPAM -lacking β subunits, but only when Ca^{2+} dependent inactivation has been suppressed with internal BAPTA.

a-d, Percentage contribution of the fast time constant of inactivation to total inactivation of Ca_v2.3 channels coexpressed with wild type and modified β subunits: β_{Sm} or the N-terminally deleted $\beta_{Sm\Delta2\text{-}44}$ (**a**), β_{1b} or the chimera NPAM-β_{1b} (**b**), β_{2a} or the chimera NPAM-β_{2a} (**c**), β_3 or the chimera NPAM-β_3 (**d**), in different intracellular buffering conditions: no buffering (open bars), buffering with 0.5 mM EGTA (green bars), and buffering with 5 mM BAPTA (blue bars). Bars represent mean ± s.e.m. $^*P < 0.05$, $^{**}P < 0.01$, $^{***}P < 0.001$ (asterisks above bars), One-way ANOVA with Bonferroni post-test (n = 3-13). Stars within bars indicate statistically significant difference between wild-type and modified β subunits for the same intracellular buffering milieu; *P < 0.05, unpaired Student's t-test. Welch's corrections were applied when the variances were significantly different.

SUPPLEMENTARY FIGURE 2. The slow component of macroscopic inactivation of Ca^{2+} currents of $Ca_v2.3$ is faster in the presence of N-terminal poly-acidic motif (NPAM)-bearing β subunits than in the presence of NPAM -lacking β subunits, but only when Ca^{2+}-dependent inactivation has been suppressed with internal BAPTA. **a-d**, Average values of the slow time constant of macroscopic inactivation (τ) for $Ca_v2.3$ channels coexpressed with wild type and modified β subunits: β_{Sm} or the N-terminally deleted $\beta_{Sm\Delta2\text{-}44}$ (**a**), β_{1b} or the chimera NPAM-β_{1b} (**b**), β_{2a} or the chimera NPAM-β_{2a} (**c**), β_3 or the chimera NPAM-β_3 (**d**). The slow τ was derived by 2-exponential fits of the inactivating portions of Ca^{2+} currents produced by HEK cells dialyzed with non-chelated solution (open bars) or with solution containing 0.5 mM EGTA (green bars) or 5 mM BAPTA (blue bars). Bars represent mean ± s.e.m. *P < 0.05, **P < 0.01, ***P < 0.001 (asterisks above bars), One-way ANOVA with Bonferroni post-test (n = 3-13). Stars within bars indicate statistically significant difference between wild-type and modified β subunits for the same intracellular buffering milieu; *P < 0.05, **P < 0.01, ***P < 0.001, unpaired Student's t-test. Welch's corrections were applied when the variances were significantly different.

SUPPLEMENTARY FIGURE 3. β subunits modulate the sensitivity of steady-state inactivation of $Ca_v2.3$ to the intracellular buffering environment.

a-i, Steady-state inactivation curves of $Ca_v2.3$ in different intracellular buffering environments expressed alone (**a**), in the presence of β_{Sm} (**b)**, the N-terminally deleted $\beta_{Sm\Delta2\text{-}44}$ (**c**), β_{1b} (**d**), the chimera NPAM-β_{1b} (**e**), β_{2a} (**f**), the chimera NPAM-β_{2a} (**g**), β_3 (**h**), or the chimera NPAM-β_3 (**i**). Ca^{2+} was the charge carrier. Intracellular conditions were: no buffer (grey circles), 0.5 mM EGTA (green triangles), or 5 mM BAPTA (blue triangles). Solid lines represent Boltzmann fits to the data. **j**, average midpoints of steady-state inactivation for the same channel subunit combinations as above in the same intracellular buffering conditions: no buffer (grey bars), 0.5 mM EGTA (green bars) and 5 mM BAPTA (blue bars). Data points represent mean ± s.e.m. (n = 3-6). *P < 0.05, **P < 0.01, ***P < 0.001 (asterisks above bars), One-way ANOVA with Bonferroni post-test. Supplementary Table 3 shows average values for midpoints of steady-state inactivation for all channel subunit combinations under various internal buffering conditions.

Table 1

Species	Acc. #	Sequence	Position
Schistosoma mansoni	AY033599	EEYDDEEYCDRADDDDDDEEEDDDEDDYKEE	17-24, 30-44
Schistosoma japonicum	CAX82734	EEYDDEEYCDRADDEDDDEEEDDDEDDYKEE	17-24, 30-44
Taenia solium	AY624029	DGEDDDED	34-41
Clonorchis sinensis	AB267713	EEDEDEEEEDEDEEEVDEEEGEYGEGEDDEEDEDEEE	23-60
Schmidtea meditteranea	EG348863	ELSFEEEKE	17-25*
Dugesia japonica	FJ483940	ELSLEEEKE	17-25

*putative position, by alignment with the corresponding sequence in *Dugesia japonica*.

Table 1. Amino acid sequence of N-terminal polyacidic clusters in β subunits of four parasitic (*Schistosome mansoni*, *S. japonicum*, *Taenia solium*, and *Clonorchis sinensis*) and two free-living platyhelminths (*Schmidtea mediterranea* and *Dugesia japonica*).

Table 2

	$\tau_{activation}$	
β subunit	- NPAM	+ NPAM
β_{Sm}	2.7 ± 0.3 (4)	2.1 ± 0 (7)
β_{1b}	2.6 ± 0.3 (5)	2.1 ± 0.2 (4)
β_{2a}	3.1 ± 0.3 (5)	1.8 ± 0.4 (3)*
β_{3}	2.2 ± 0.1 (3)	1.5 ± 0.1 (3)*

Table2. Activation time constants ($\tau_{activation}$) of Ba^{2+} currents produced by $Ca_v2.3$ channels in combination with wild type and mutated β subunits from *Schistosoma mansoni* (β_{Sm}) and mammals. $\tau_{activation}$ was derived from single exponential fits to the activating portion of the inward currents. The N-termini of mammalian chimeric β subunits corresponds to the N-terminus of β_{Sm}, which contains a long polyacidic motif of 15 glutamate and aspartate residues (NPAM). Data represent mean ± s.e.m. N is shown in parentheses. * $p < 0.05$, unpaired Student t-test, with respect to the same β subunit lacking NPAM. N = 3-7.

Figure 1

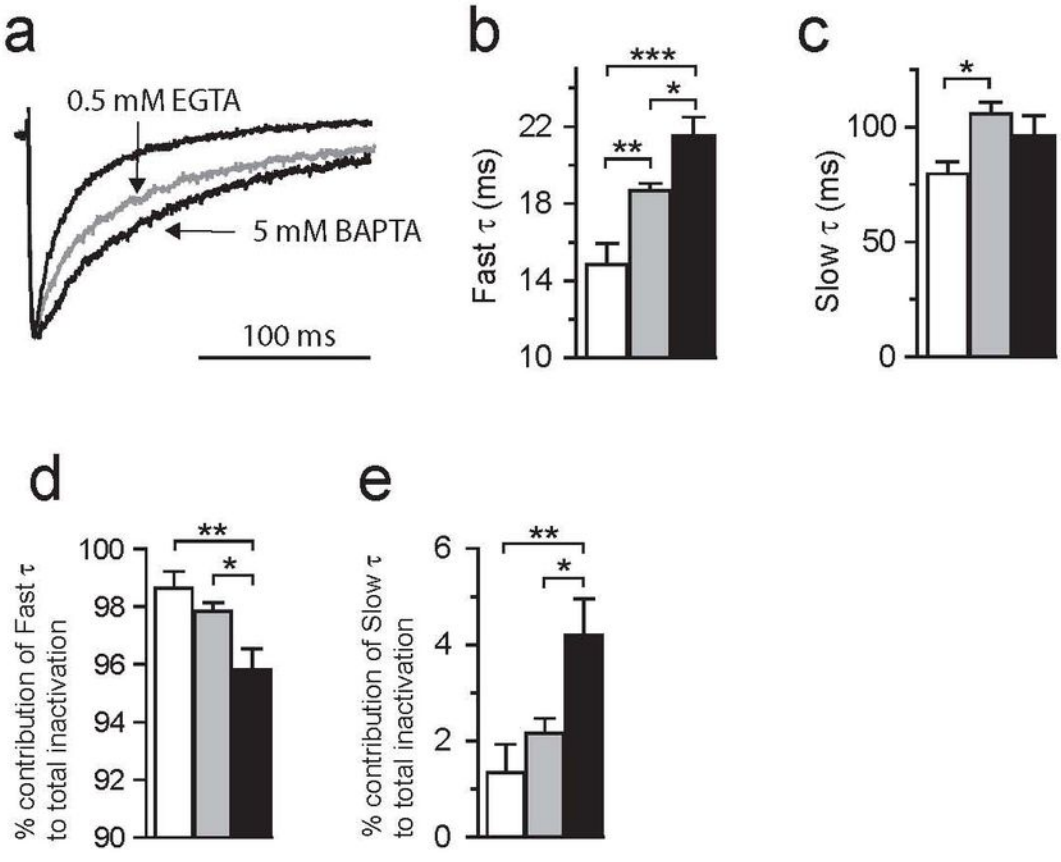
a
0.5 mM EGTA
5 mM BAPTA
100 ms
b
***
**
*
Fast τ (ms)
22
18
14
10
c
*
Slow τ (ms)
100
50
0
d
**
*
% contribution of Fast τ to total inactivation
100
98
96
94
92
90
e
**
*
% contribution of Slow τ to total inactivation
6
4
2
0

Figure 2

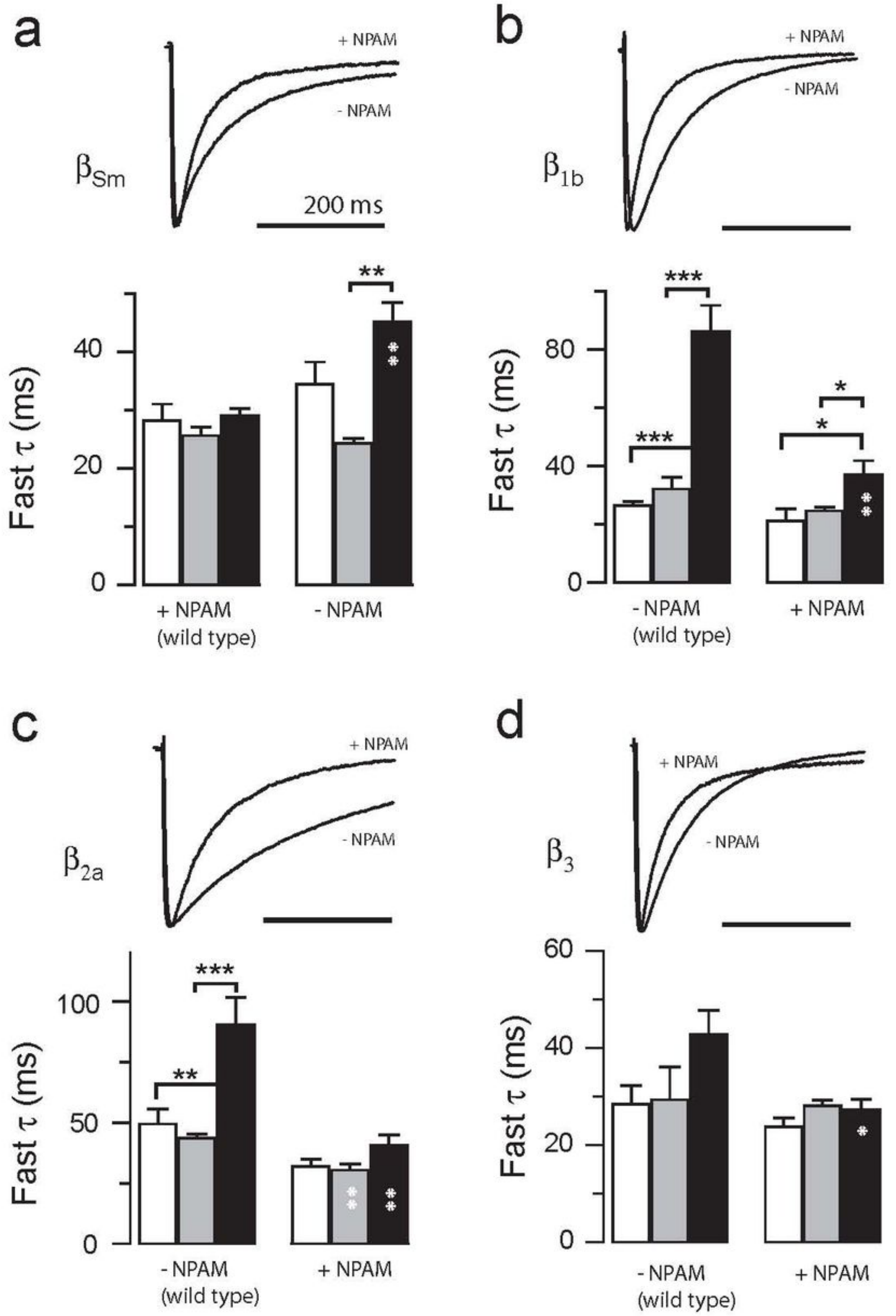

a
+ NPAM
- NPAM
βSm
200 ms
**
Fast τ (ms)
40
20
0
+ NPAM
(wild type)
- NPAM
b
+ NPAM
- NPAM
β1b
***
*
Fast τ (ms)
80
40
0
- NPAM
(wild type)
+ NPAM
c
+ NPAM
- NPAM
β2a
***
**
Fast τ (ms)
100
50
0
- NPAM
(wild type)
+ NPAM
d
+ NPAM
- NPAM
β3
60
40
20
0
Fast τ (ms)
- NPAM
(wild type)
+ NPAM

Figure 3

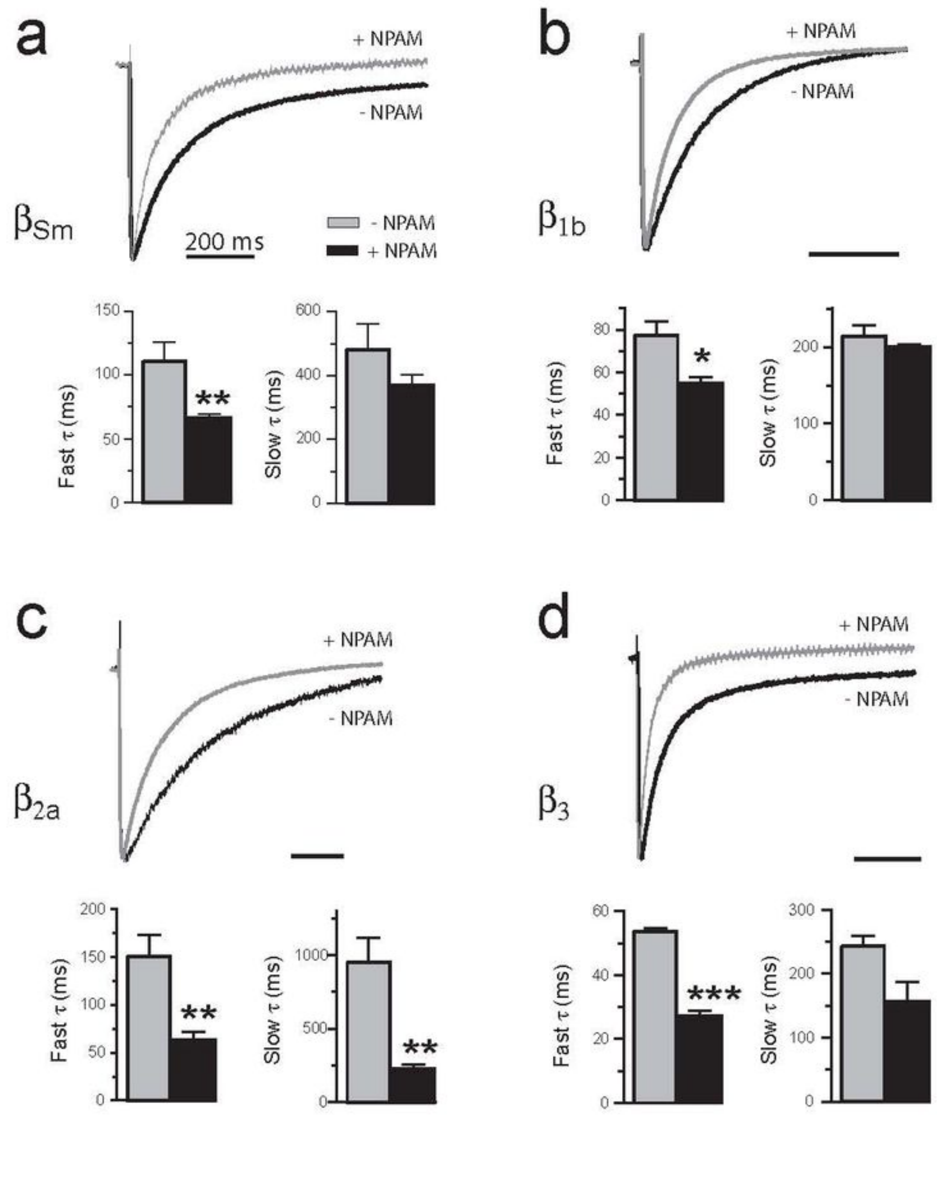

a
+ NPAM
- NPAM
βSm
200 ms
- NPAM
+ NPAM
Fast τ (ms)
**
Slow τ (ms)
b
+ NPAM
- NPAM
β1b
Fast τ (ms)
*
Slow τ (ms)
c
+ NPAM
- NPAM
β2a
Fast τ (ms)
**
Slow τ (ms)
**
d
+ NPAM
- NPAM
β3
Fast τ (ms)
***
Slow τ (ms)

Figure 4

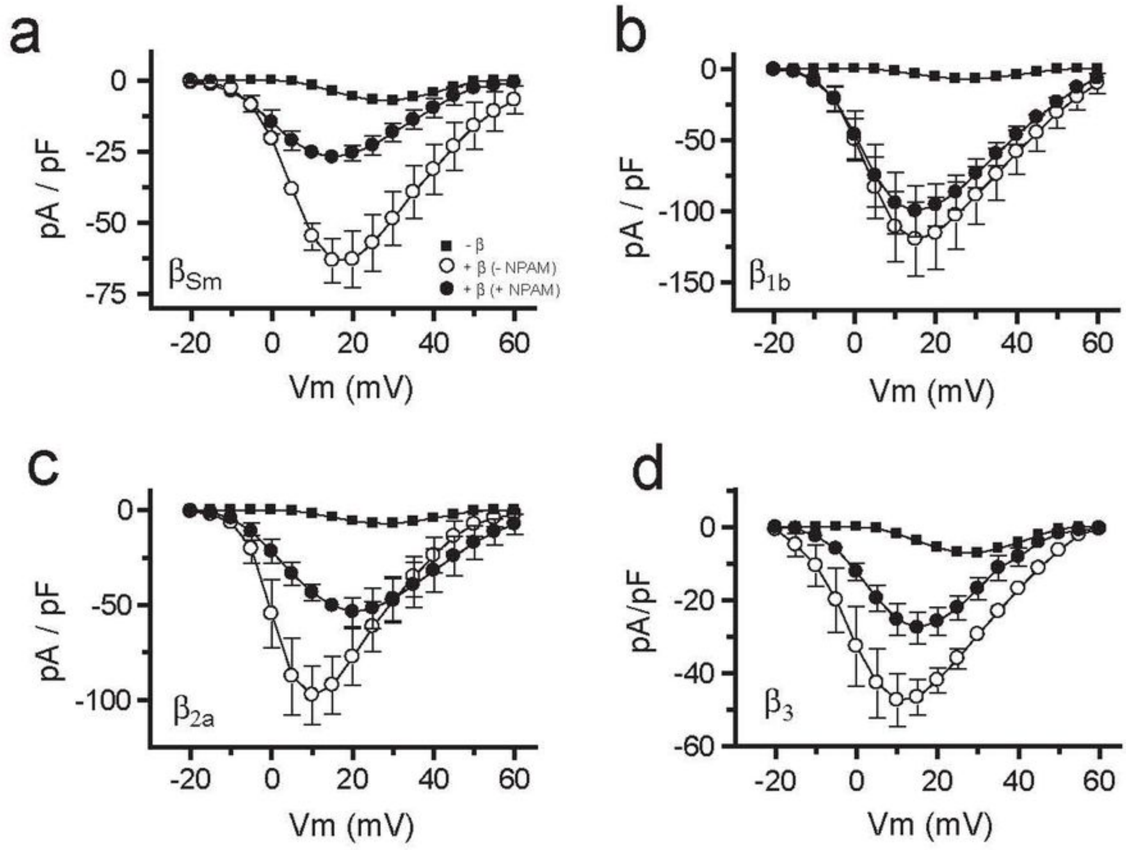

a
b
c
d
pA / pF
pA/pF
Vm (mV)
- β
+ β (- NPAM)
+ β (+ NPAM)
β_{Sm}
β_{1b}
β_{2a}
β_{3}

Figure 5

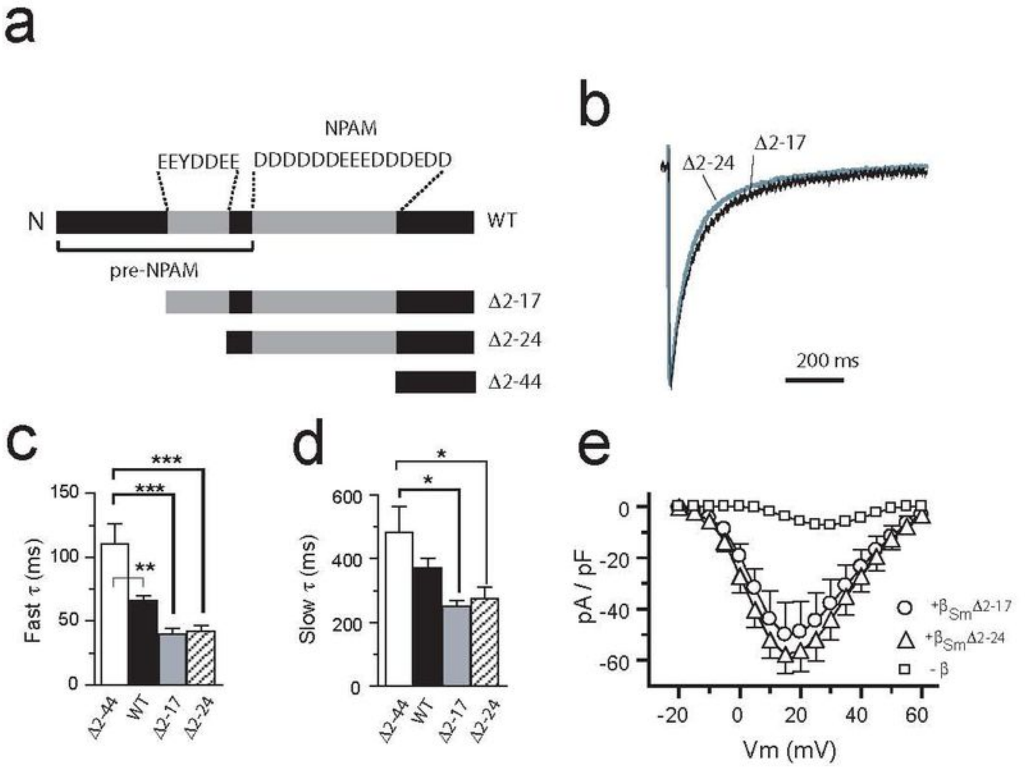

a
NPAM
EEYDDEE
DDDDDDEEEDDDEDD
N
WT
pre-NPAM
Δ2-17
Δ2-24
Δ2-44
b
Δ2-24
Δ2-17
200 ms
c
Fast τ (ms)
150
100
50
0
***
***
**
Δ2-44
WT
Δ2-17
Δ2-24
d
Slow τ (ms)
600
400
200
0
*
*
Δ2-44
WT
Δ2-17
Δ2-24
e
pA / pF
0
-20
-40
-60
-20
0
20
40
60
Vm (mV)
+βSmΔ2-17
+βSmΔ2-24
- β

Figure 6

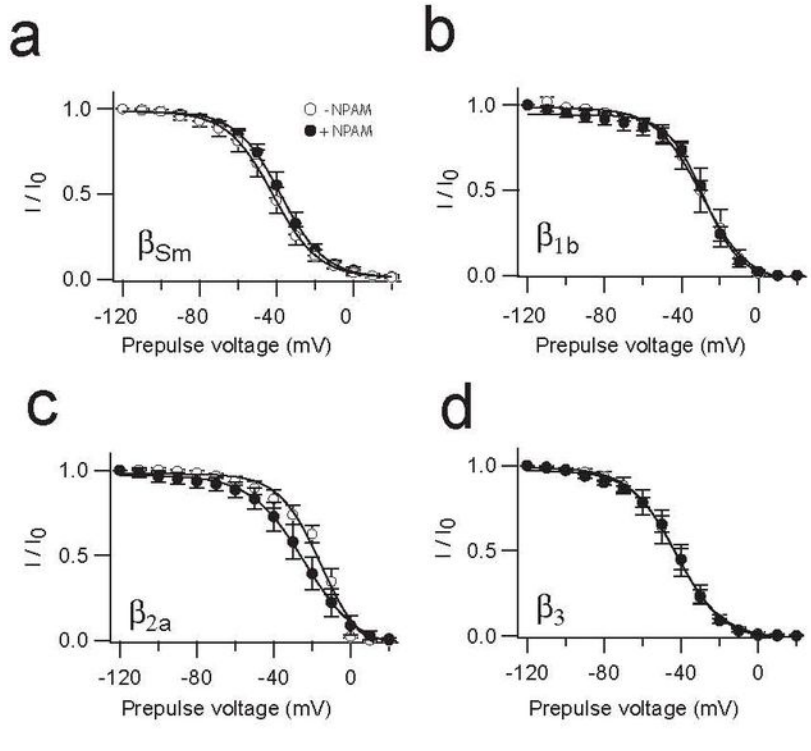

a
b
c
d
1.0
0.5
0.0
I / I0
-120
-80
-40
0
Prepulse voltage (mV)
-NPAM
+NPAM
βSm
β1b
β2a
β3